

# Epitaxial Growth of Magnesia Films on Single Crystalline Magnesia Substrates by Atmospheric-Pressure Chemical Vapor Deposition

Keiji Komatsu<sup>1</sup>, Pineda Marulanda David Alonso<sup>1</sup>, Nozomi Kobayashi<sup>1</sup>, Ikumi Toda<sup>1</sup>, Shigeo Ohshio<sup>1</sup>,  
Hiroyuki Muramatsu<sup>1</sup> & Hidetoshi Saitoh<sup>1</sup>

<sup>1</sup> Department of Materials Science and Technology, Nagaoka University of Technology, Japan

Correspondence: Keiji Komatsu, Department of Materials Science and Technology, Nagaoka University of Technology, 1603-1 Kamitomioka, Nagaoka, Niigata 940-2188, Japan. TEL: 81-258-479-379 E-mail: Keiji\_Komatsu@mst.nagaokaut.ac.jp

Received: December 14, 2015 Accepted: January 19, 2016 Online Published: January 31, 2016

doi:10.5539/jmsr.v5n2p56

URL: <http://dx.doi.org/10.5539/jmsr.v5n2p56>

## Abstract

MgO films were epitaxially grown on single crystal MgO substrates by atmospheric-pressure chemical vapor deposition (CVD). Reciprocal lattice mappings and X-ray reflection pole figures were used to evaluate the crystal quality of the synthesized films and their epitaxial relation to their respective substrates. The X-ray diffraction profiles indicated that the substrates were oriented out-of-plane during MgO crystal growth. Subsequent pole figure measurements showed how all the MgO films retained the substrate in-plane orientations by expressing the same pole arrangements. The reciprocal lattice mappings indicated that the whisker film showed a relatively strong streak while the continuous film showed a weak one. Hence, highly crystalline epitaxial MgO thin films were synthesized on single crystal MgO substrates by atmospheric-pressure CVD.

**Keywords:** epitaxial growth, magnesia oxide, atmospheric-pressure chemical vapor deposition, single crystalline magnesia substrate

## 1. Introduction

Magnesium oxide (MgO) has attracted the attention of many researchers for application to semiconductors (Bian et al., 2004; Henyk et al., 2005; Nam et al., 2006; Tamboli et al., 2009; Nakano et al., 2004). MgO shows an excellent antispattering property, a high secondary electron emission coefficient, and visible light permeability. Many researchers have used metal-organic chemical vapor deposition (MOCVD), (Fujita et al., 1999; Zeng et al., 1996; Sung et al., 2000) laser ablation (Chen et al., 2004), and electron beam evaporation (P. O'Connor Casey et al., 2009) to synthesize epitaxial MgO films. In addition, MgO films showing various orientations and morphologies have been deposited using various techniques (Raj et al., 2010).

Atmospheric-pressure chemical vapor deposition (CVD) is a method of depositing high-quality metal oxide films onto various substrates at atmospheric pressure and without requiring a vacuum system (Saitoh, Okada, & Ohshio, 2002; Saitoh, Takano, Kawaguchi, Washio, Ohshio, & Akasaka, 2009; Akasaka et al., 2013; Sugata et al., 2003; Satoh et al., 2002; Satou et al., 1999; Saitoh, Fukada, & Ohshio, 2003; Tokita, Tanaka, & Ohshio, 2003; Tokita, Tanaka, & Saitoh, 2000). Further, the atmospheric-pressure CVD apparatus is inexpensive and can be used to deposit uniform, homogeneous, dense films showing high coverage, tunable chemical compositions and morphologies, and no uncoated "hidden areas." For example, atmospheric-pressure CVD has been used to synthesize MgO/ZnO heterojunction film on single crystalline alumina (Saitoh, Okada, & Ohshio, 2002), and In<sub>2</sub>O<sub>3</sub> heteroepitaxial film on single crystal yttria-stabilized zirconia (YSZ) substrates (Sugata et al., 2003). Furthermore, it has been used to synthesize functionality-oriented metal oxide films such as Y<sub>2</sub>O<sub>3</sub>-based phosphors (Satoh et al., 2002) and ZnO whiskers as electron beam sources (Satou et al., 1999; Saitoh, Fukada et al., 2003) and has recently been used to synthesize MgO whiskers, which show potential for application as an electron source (Saitoh & Takano, 2009; Akasaka et al., 2013).

In this study, atmospheric-pressure CVD was used to deposit epitaxial MgO films onto single crystalline magnesia substrates. Epitaxial growth of MgO films were revealed from three crystallographic approaches. Magnesium acetylacetonate (Mg(C<sub>5</sub>H<sub>7</sub>O<sub>2</sub>)<sub>2</sub>) were used as raw material for the MgO films. First, microstructure of the deposited films was observed. Next, crystalline structures (out-of-plane and in-plane) for deposited films were revealed by

XRD, pole figure, and reciprocal lattice mapping measurements. Crystallographic analysis revealed that the films were epitaxial.

## 2. Experimental Work

We used an atmospheric-pressure CVD apparatus to deposit the films onto  $10 \times 10 \times 0.5$ -mm<sup>3</sup> single crystalline magnesia (100), (111), and (100) substrates (Dalian Keri Optoelectronic Technology Co., Ltd.). The schematic of the apparatus is shown in Figure 1. Nitrogen (N<sub>2</sub>) was used as the carrier gas, constantly flowing at 1.5 L/min. Magnesium acetylacetonate (Mg(C<sub>5</sub>H<sub>7</sub>O<sub>2</sub>)<sub>2</sub>; Nacalai Tesque, Inc., Japan) was used as the precursor raw material to deposit the MgO films; 2 g of the precursor material were put into an alumina boat, which was placed inside the evaporation chamber for film deposition. The pipe and the nozzle through which the vapor must travel between the evaporation chamber and the substrate were heated to 240°C to prevent the vaporized precursor from recrystallizing. The substrate was placed on a heating plate at 650°C. The temperature of the pipes and the chamber and the flow of the carrier gas were allowed to stabilize for 1 h between experiments. The distance between the nozzle and the substrate was constantly maintained at 7.5, 10, or 15 mm. All the MgO films were continuously deposited onto single crystalline MgO substrates for 6.4 h. Table 1 shows the experimental conditions for Samples 1-6.

Table 1. Experimental conditions for Samples 1-6

Sample	MgO substrate Orientation	Nozzle-substrate distance, <i>d</i> (mm)
Sample 1	(100)	7.5
Sample 2	(100)	10.0
Sample 3	(100)	15.0
Sample 4	(111)	7.5
Sample 5	(111)	10.0
Sample 6	(111)	15.0

## 3. Characterization

The surface microstructures and cross-sectional morphologies of deposited films were observed and the film thicknesses were measured using scanning electron microscopy (SEM; JSM6700F, JEOL) operated at 5-kV acceleration. X-ray diffraction (XRD, MO3XHF, Mac Science Co., Ltd.) was used to determine the crystal structure and growth direction of the samples. Pole figures were also measured to investigate the in-plane orientation. The incident angle,  $2\theta$ , was set to the strongest diffraction line obtained in the  $\theta$ - $2\theta$  scan and was kept constant. The  $\alpha$  angle was set to tilt between 15 and 80° in 0.5° steps, and the  $\delta$  angle was scanned in circles from 0 to 360° at 250°/min while the diffracted X-rays were collected and measured. The X-ray was produced by a voltage and current of 30 kV and 30 mA, respectively. Furthermore, a three-axis RIGAKU 9-kW diffractometer equipped with the SMARTLAB and NewInfo analysis software was used to measure reciprocal space mappings for the deposited films. The measurement was performed centered on the asymmetric reciprocal lattice point (-204), where  $2\theta = 109.72^\circ$  and was offset by  $\omega = -28.39^\circ$ . The  $2\theta$  angle was varied between 105.00 and 115.45° in 0.05° steps, and  $\omega$  was tilted between -31.5 and -21.5° in 0.05° steps. The samples were scanned at 12°/min. The Cu-K $\alpha$  X-ray ( $\lambda = 1.54 \text{ \AA}$ ) was generated by a 50 kV voltage and 200 mA current.

## 4. Results and Discussion

### 4.1 Morphological Study

Atmospheric-pressure CVD enables films composed of various forms of metal oxide crystals to be synthesized by widely changing the degree of supersaturation during film deposition. For instance, the crystal morphology destabilizes; that is, continuous film surfaces roughen with increasing supersaturation (Tokita, Tanaka, & Ohshio, 2003; Tokita, Tanaka, & Saitoh, 2000). The surface and cross-sectional SEM images of the deposited films are shown in Figures 2 and 3. Figure 2 shows SEM images of the Samples 1-3 films deposited onto the MgO (100) substrates. Sample 1 (nozzle-substrate distance was 7.5 mm) showed an amorphous mass with no discernible geometrical features (Figure 2(a) and (b)). The deposited film was approximately 1  $\mu\text{m}$  thick. Sample 2 (nozzle-substrate distance was 10 mm) was a 0.2-0.5  $\mu\text{m}$ -thick film showing an orderly arrangement of squares oriented in the same direction (Figures 2(c) and (d)). Sample 3 (nozzle-substrate distance was 15 mm) shows how these squares were actually the tips of  $\sim 0.5$ - $\mu\text{m}$ -thick column-like whiskers, which grew perpendicular to the surface of the substrate and in tight mutually lateral contact; that is, the whiskers were in contact with the

surrounding ones without any void spaces between them, forming a tight column-whisker-structured continuous film (Figures 2(e) and (f)). Crystalline films usually contain various crystals, which exhibit different appearances and habits (i.e. crystal orientation direction and morphology). MgO films deposited using various methods onto various substrates have shown different characteristics; hence, we investigated the influence of various substrate orientations on the film microstructures. Figure 3 shows surface and cross-sectional images of the Samples 4–6 films deposited onto (111) MgO substrates (Oumi et al., 2003; Lee et al., 2000). Figures 3(a) and (b) show the surface and cross-sectional SEM images of Sample 4 (nozzle-substrate distance was 7.5 mm), respectively. The  $\sim 1\text{-}\mu\text{m}$ -thick film showed a continuous surface morphology. Sample 5 (nozzle-substrate distance was 10 mm) showed  $0.1\text{--}0.4\ \mu\text{m}$ -thick laterally arranged triangular structures (Figures 3(c) and (d)). The cross-sectional SEM image shows  $2\text{-}\mu\text{m}$ -high perpendicular column-like whiskers. Sample 6 (nozzle-substrate distance was 15 mm) contained  $\sim 2\ \mu\text{m}$ -thick triangle-like whiskers (Figure 3(e) and (f)). These results indicate that the microstructures on deposited films differed according to the substrate orientation and the nozzle-substrate distance.

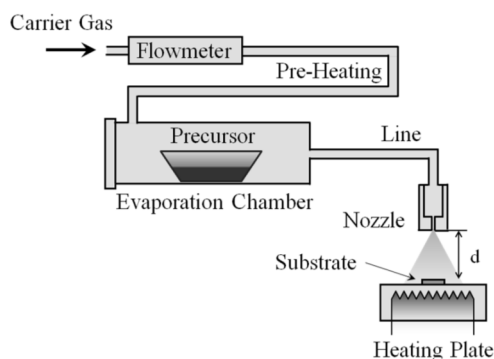


Figure 1. Schematic of atmospheric CVD apparatus

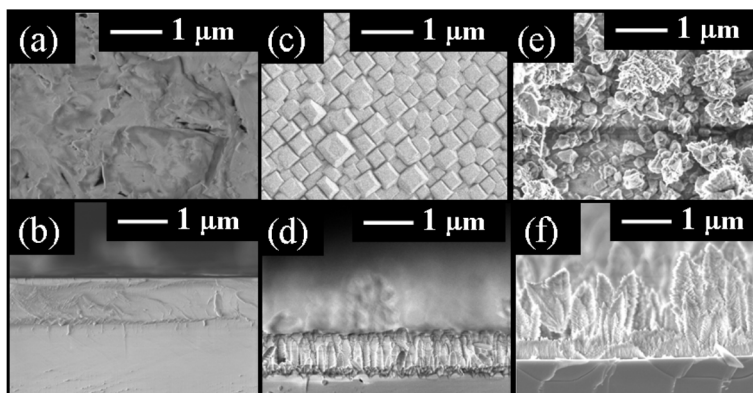


Figure 2. Surface and cross-sectional SEM images of Samples 1–3 films deposited onto single crystalline MgO (100) substrates: (a), (c), and (e) are surface SEM images and (b), (d), and (f) are cross-sectional SEM images

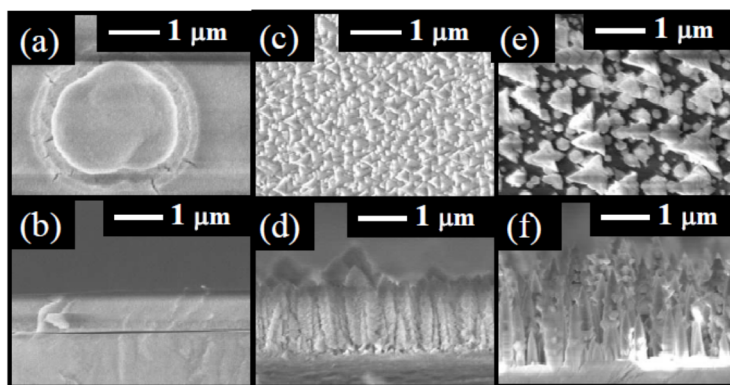


Figure 3. Surface and cross-sectional SEM images of Samples 4–6 films deposited onto single crystalline MgO (111) substrates: (a), (c), and (e) are surface SEM images and (b), (d), and (f) are cross-sectional SEM images

#### 4.2 Crystal Structure (Out-of-Plane) Analysis

The sample crystallinities were then investigated based on the  $\theta$ -2 $\theta$  XRD measurements, as shown in Figures 4 and 5. All the obtained XRD profiles showed a single peak in the range  $2\theta = 20$ – $75^\circ$ . A single peak at  $42.96^\circ$ , assigned to the (200) diffraction line for MgO crystal (ICDD card No.: 01-071-1176), was detected for the films deposited onto the MgO (100) substrates. In contrast, a single peak at  $37.44^\circ$ , assigned to the (111) diffraction line for the MgO crystal, was detected for the films deposited onto the MgO (111) substrates. We estimated the full width at half maximum (FWHM) for each diffraction peak and the results are listed in Table 2. The FWHMs for the deposited films were almost identical to those for the corresponding MgO (100) and (111) substrates. The  $\theta$ -2 $\theta$  XRD profiles indicated that the samples were oriented in the out-of-plane direction (Kobayashi, 2010; Tokita, Tanaka, & Mitsunaga, 2009). Hence, the profiles represent out-of-plane-oriented MgO film growth and imply that the films preferentially grew oriented in the direction of the MgO substrate plane.

Table 2. FWHMs for Samples 1–6, estimated from XRD profiles

Sample	FWHM (nm)
Sample 1	0.35
Sample 2	0.26
Sample 3	0.26
Sample 4	0.25
Sample 5	0.20
Sample 6	0.22
MgO (100) substrate	0.26
MgO (111) substrate	0.24

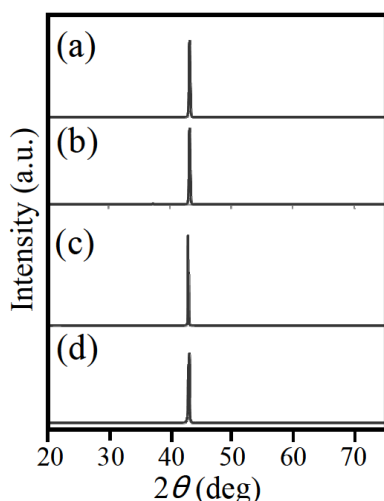


Figure 4. XRD profiles for Samples 1–3 films deposited onto single crystalline MgO (100) substrates

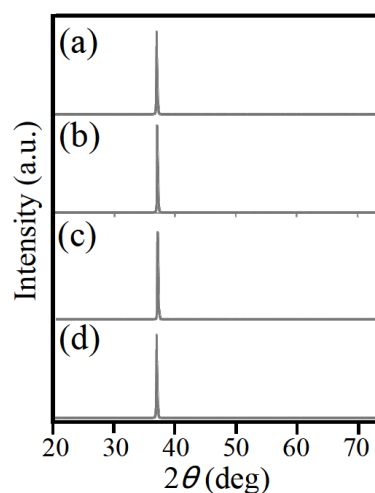


Figure 5. XRD profiles for Samples 4–6 films deposited onto single crystalline MgO (111) substrates

#### 4.3 Crystal Orientation (In-Plane) Analysis

Pole figures were measured to investigate the in-plane orientation of the films deposited at the different nozzle-substrate distances and were plotted in stereographic projections (Figures 6 and 7). According to previous reports on the equilibrium formation of rock salt crystals, MgO films could face the lower-energy direction while retaining the preferred growth direction (Chudzik et al., 2001; Maksimov et al., 2008). The pole figures and intensity diagrams for the MgO (100) substrate and for the films deposited onto MgO (100) substrates are shown in Figure 6. A set of four poles appeared at  $\alpha = 19^\circ$  mutually separated by  $90^\circ$  in four-fold symmetry. Another set of eight poles was observed at  $\alpha = 42^\circ$ , each separated by  $45^\circ$  from the adjacent one in eight-fold symmetry. The four-fold symmetrically arranged poles at  $\alpha = 19^\circ$  were assigned to the 110-pole set of the MgO crystal, and the

eight-fold symmetrically arranged poles at  $\alpha = 42^\circ$  were assigned to the 221-pole set of the MgO crystal. The intensity diagrams revealed weak poles for the sample deposited at 7.5 mm, which were dimmer than those for the substrate and for the films deposited at 10 and 15 mm (Figure 6(f)-(h)). The pole figures and intensity diagrams for the MgO (111) substrate and for the films deposited onto MgO (111) substrates are shown in Figure 7. A single set of three poles was observed at  $\alpha = 21^\circ$ , mutually separated by  $120^\circ$  in three-fold symmetry. The observed three-fold symmetrically arranged poles at  $\alpha = 21^\circ$  were assigned to the 110-pole set on the 111-plane projection. Pole figure analysis has previously been used to show the biaxial textures of MgO thin films synthesized on amorphous glass substrates (Cho et al., 2003). Thus, the in-plane orientations of the substrates were retained during deposition, as shown by the constant pole distribution for Samples 1–6. The epitaxial growth of MgO films can be ensured during atmospheric-pressure CVD, even when changing the deposition distance.

Reciprocal lattice point measurements can be used to estimate the lattice parameter expansion and mosaicity of films deposited onto various substrates (Krop et al., 2014; Hwang et al., 1996). Hence, we measured the reciprocal lattice points for the films deposited onto the MgO (100) and (111) substrates, as shown in Figures 8 and 9. The topological representation of the reciprocal map for Sample 2 is presented in Figure 8. A very strong singular peak was detected centered in the measured space of the  $(-204)$  reciprocal lattice point, indicating that the substrate and film were strongly oriented. Figure 9 shows the reciprocal space for Sample 2 transformed into the Qx-Qz space in a two-dimensional color diagram. The ring band crossing the two-dimensional diagram through the peak in the radial direction is less prominent than the ring band for Sample 3 (Figures 8(b) and 9(b)), indicating that the Sample 3 deposited film showed reduced mosaicity or a more-organized structure closer to perfect epitaxy. A higher degree of crystalline orientation was therefore achieved by setting the nozzle-substrate distance to 10 mm, where the deposited film grew more uniformly in the c-axis direction (perpendicular to the substrate surface). The SEM images readily show the higher growth uniformity of the column-like whisker film. Reciprocal space mappings have previously been reported for epitaxial MgO films grown on SrTiO<sub>3</sub> substrate (Kannedy et al., 1999). The mappings clearly indicate the lattice symmetry and the tilt- and strain-free lattice of the MgO film. In contrast, the reciprocal space mapping for Sample 5 showed a very strong singular peak centered in the measured space of the (422) reciprocal lattice point, as shown in Figure 8(c). From the Qx-Qz space diagram, the deposited film showed a high degree of mosaicity, identical to the MgO (100) substrate. Hence, highly crystalline epitaxial MgO thin films were synthesized on single crystal MgO substrates by atmospheric-pressure CVD.

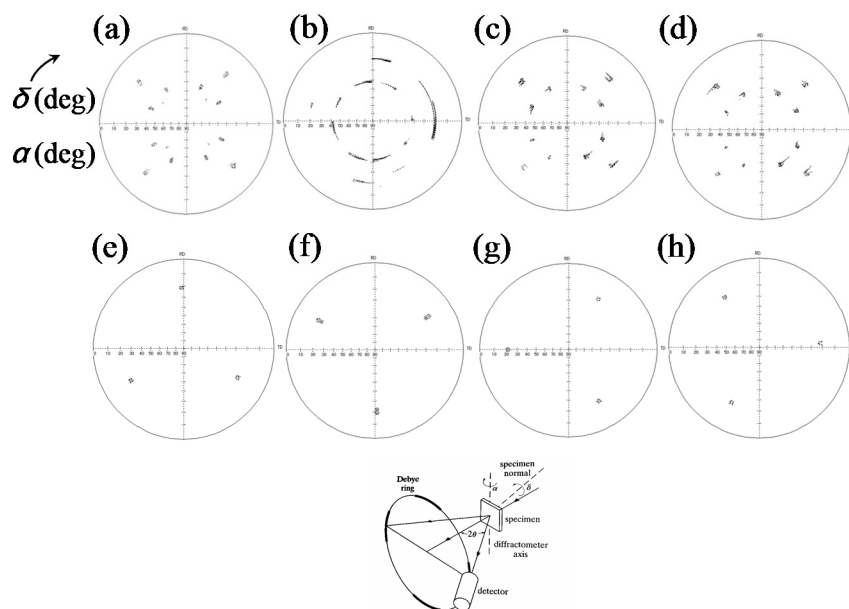


Figure 6. Pole figures for (a) MgO (100) and (e) MgO (111) substrates and for ((b)-(d)) Samples 1–3 and ((f)-(h)) Samples 4–6 films deposited onto MgO (100) and (111) substrates by atmospheric pressure CVD. Schematic shows how  $\alpha$  and  $\delta$  are defined for specimens

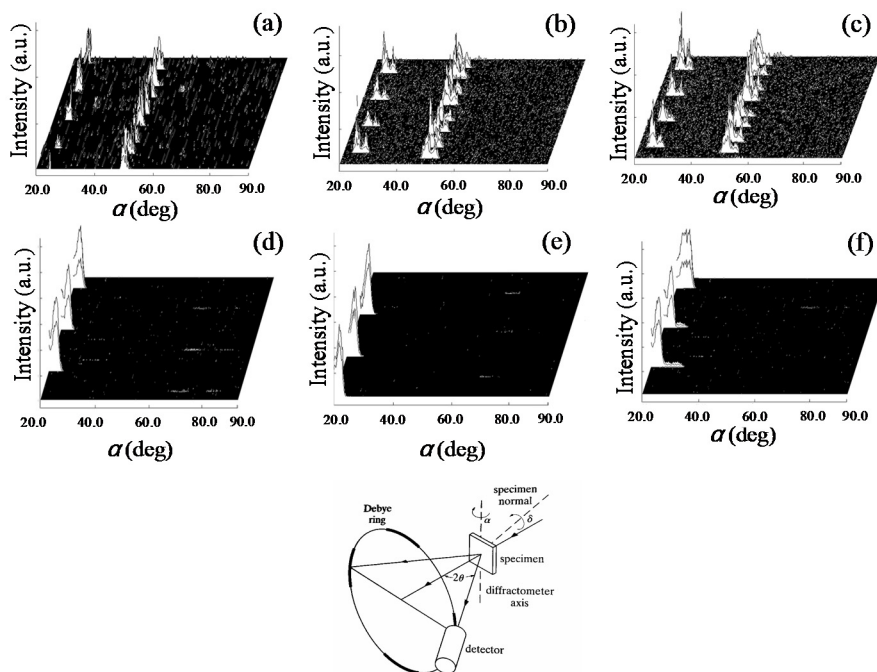


Figure 7. Pole intensity diagrams for (a) Sample 1, (b) Sample 2, (c) Sample 3, (d) Sample 4, (e) Sample 5, and (f) Sample 6 MgO films deposited onto MgO (100) and (111) substrates. Schematic shows how  $\alpha$  and  $\delta$  are defined for specimens

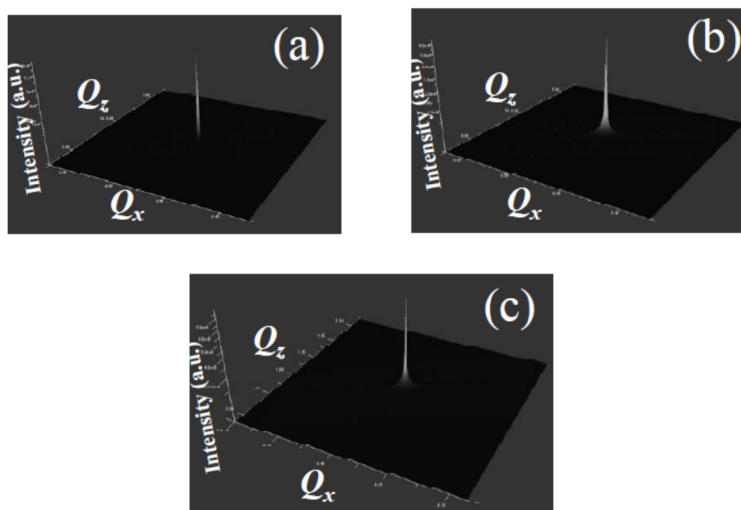


Figure 8. (a), (b) Topologies of reciprocal lattice mapping on  $(-204)$  reciprocal lattice point for Samples 2 and 3 MgO films, respectively, deposited onto MgO (100) substrates. (c) Topology of reciprocal lattice mapping on  $(422)$  reciprocal lattice point for Sample 5 MgO film deposited onto MgO (100) substrate

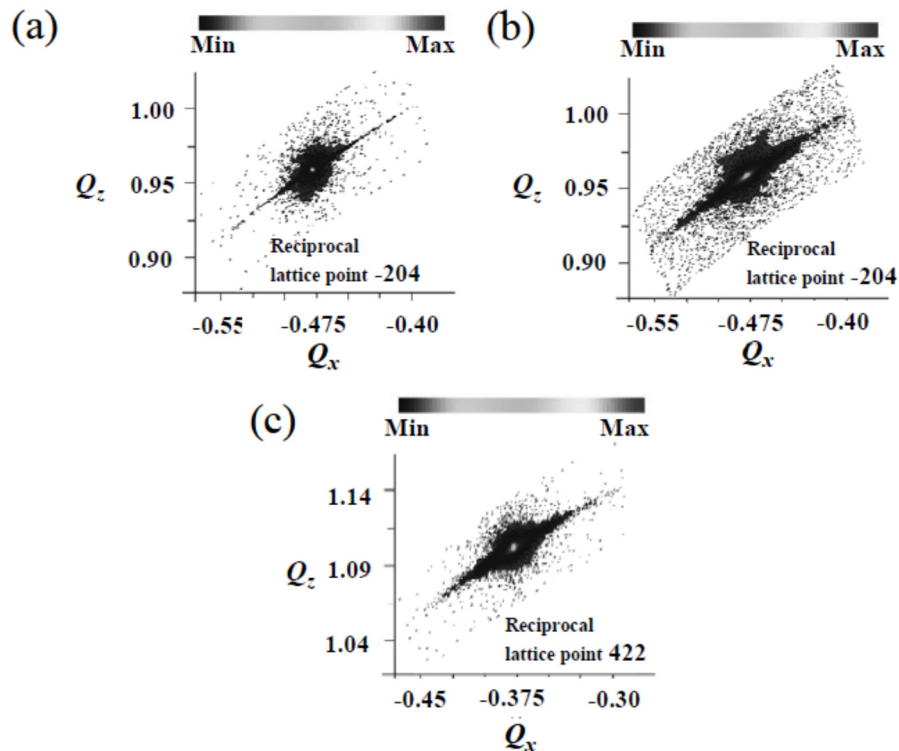


Figure 9. Two-dimensional representations of reciprocal space measurements on momentum-transfer plane ( $Q_x$ ,  $Q_z$ ) for (a) Sample 2, (b) Sample 3, and (c) Sample 5MgO films deposited onto MgO (100) and (111) substrates

## 5. Conclusion

Epitaxial MgO films were synthesized on single crystal MgO substrates by atmospheric-pressure CVD. The out-of-plane and in-plane orientations of their respective substrates were determined using XRD, pole figure measurements, and reciprocal lattice mapping. The reciprocal lattice mappings indicated that the mosaicity of the deposited MgO films depended on the film morphology.

## Acknowledgment

We appreciate as well the support and expert advice of the staff at the Analysis and Instrumentation center at Nagaoka University of Technology, especially professor Hiroshi Matsubara and Hideyuki Toyota, whose contribution to the reciprocal mapping measurement and analyses were invaluable.

## References

- Bian, J. M., Li, X. M., Chen, T. L., Gao, X. D., & Yu, W. D. (2004). Preparation of high quality MgO thin films by ultrasonic spray pyrolysis. *Applied Surface Science*, 228, 297–301. <http://dx.doi.org/10.1016/j.apsusc.2004.01.020>
- Henryk, M., Beck, K.M., Engelhard, M.H., Joly, A.G., Hess, W. P., & Dickinson, J. T. (2005). Surface electronic properties and site-specific laser desorption processes of highly structured nanoporous MgO thin films. *Surface Science*, 593, 242–247. <http://dx.doi.org/10.1016/j.susc.2005.06.090>
- Nam, K.S., Lee, H.J., Lee, S. H., Lee, G.H., Song, Y.S., & Lee, D.Y. (2006). The effect of an atmospheric pressure plasma treated MgO layer on the discharge performance of an AC plasma display panel. *Surface and Coatings Technology*, 201, 2567–2572. <http://dx.doi.org/10.1016/j.surfcoat.2006.04.065>
- Tamboli, S.H., Patil, R.B., Kamat, S.V., Puri, V., & Puri, R.K. (2009). Modification of optical properties of MgO thin films by vapour chopping. *Journal of Alloys and Compounds*, 477, 855–859. <http://dx.doi.org/10.1016/j.jallcom.2008.11.011>
- Nakano, T., Fujimoto, T., & Baba, S. (2004). Measurement of surface roughness and ion-induced secondary electron emission coefficient of MgO films prepared by high-pressure sputter deposition. *Vacuum*, 74, 595–599. <http://dx.doi.org/10.1016/j.vacuum.2004.01.064>

- Fujii, E., Tomozawa, A., Torii, H., Takayama, R., Nagaki, M., & Narusawa, T., (1999). Preferred orientations and microstructure of MgO films prepared by plasma-enhanced metalorganic chemical vapor deposition. *Thin Solid Films*, 352, 85–90. [http://dx.doi.org/10.1016/S0040-6090\(99\)00343-0](http://dx.doi.org/10.1016/S0040-6090(99)00343-0)
- Zeng, J.M., Wang, H., Shang, S.X., Wang, Z., & Wang, M. (1996). Preparation and characterization of epitaxial MgO thin film by atmospheric-pressure metalorganic chemical vapor deposition. *Journal of Crystal Growth*, 169, 474–479. [http://dx.doi.org/10.1016/S0022-0248\(96\)00411-3](http://dx.doi.org/10.1016/S0022-0248(96)00411-3)
- Sung, M.M., Kim, C., Kim, C. G., & Kim, Y. (2000). Epitaxial growth of MgO films on Si(111) by metal organic chemical vapor deposition. *Journal of Crystal Growth*, 210, 651–654. [http://dx.doi.org/10.1016/S0022-0248\(99\)00847-7](http://dx.doi.org/10.1016/S0022-0248(99)00847-7)
- Chen, T., Li, X. M., & Zhang, S. (2004). Enhanced strain relaxation induced by epitaxial layer growth mode of MgO thin films. *Solid State Communications*, 131, 523–526. <http://dx.doi.org/10.1016/j.ssc.2004.06.016>
- Casey, P. O'Connor, E., Long, R., Brennan, B. Krasnikov, S. A., O'Connell, D., Hurley, P.K., & Hughes, G. (2009). Growth, ambient stability and electrical characterization of MgO thin films on silicon surfaces. *Microelectronic Engineering*, 86, 1711–1714. <http://dx.doi.org/10.1016/j.mec.2009.03.046>
- Raj, A.M.E., Jayachandran, M., & Sanjeeviraja, C. (2010). Fabrication techniques and material properties of dielectric MgO thin films—A status review. *CIRP Journal of Manufacturing Science and Technology*, 2, 92–113. <http://dx.doi.org/10.1016/j.cirpj.2010.02.003>
- Saitoh, H., Okada, Y., & Ohshio, S. (2002). Synthesis of MgO/ZnO hetero-epitaxial whiskers using chemical vapor deposition operated under atmospheric pressure. *Journal of Material Science*, 37, 4597–4602. <http://dx.doi.org/10.1023/A:1020696215411>
- Saitoh, H., Takano, A., Kawaguchi, S., Washio, T., Ohshio, S., & Akasaka, H. (2009). Discharge property between magnesium oxide films with various true densities. *Journal of the Ceramic Society of Japan*, 117, 780–782. <http://doi.org/10.2109/jcersj2.117.780>
- Akasaka, H., Matsuda, K., Minami, R., Kiyokawa, T., Takano, A., Ohshio, S., ... Saitoh, H. (2013). Structured MgO coated electrodes to reduce the inception voltage. *Thin Solid Films*, 534, 465–469.
- Sugata, H., Ohshio, S., & Saitoh, H. (2003). Heteroepitaxy of In<sub>2</sub>O<sub>3</sub> whiskers fabricated on single crystalline (001) yttrium stabilized zirconia. *Japanese journal of applied physics*, 42, 2786–2790. <http://doi.org/10.1143/JJAP.42.2786>
- Satoh, Y., Ohshio, S., & Saitoh, H. (2002). Photoluminescence properties of Y<sub>2</sub>O<sub>3</sub>:Eu whiskers with preferential <100> orientation. *Japanese journal of applied physics*, 41, L1253–L1255. <http://doi.org/10.1143/JJAP.41.L1253>
- Satou, M., Tanaka, N., Ueda, Y., Ohshio, S., & Saitoh, H. (1999). Epitaxial growth of zinc oxide whiskers by chemical-vapor deposition under atmospheric pressure, *Japanese journal of applied physics*, 38, L586–L589. <http://doi.org/10.1143/JJAP.38.L586>
- Saitoh, H., Fukada, Y., & Ohshio, S. (2003). Zinc oxide whiskers with intense ultraviolet emission, *Journal of the Ceramic Society of Japan*, 111, 1–3. <http://doi.org/10.2109/jcersj.111.1>
- Tokita, S., Tanaka, N., Ohshio, S., & Saitoh, H. (2003). Photo-induced Surface reaction of highly oriented anatase polycrystalline films synthesized using a CVD apparatus operated in atmospheric regime, *Journal of the Ceramic Society of Japan*, 111, 433–435. <http://doi.org/10.2109/jcersj.111.433>
- Tokita, S., Tanaka, N., & Saitoh, H. (2000). High-rate epitaxy of anatase films by atmospheric chemical vapor deposition, *Japanese journal of applied physics*, 39, L169–L171. <http://doi.org/10.1143/JJAP.39.L169>
- Oumi, K., Matsumoto, H., Kashiwagi, K., & Murayama, Y. (2003). MgO thin films for plasma display panel formed by plasma process. *Surface and Coatings Technology*, 169–170, 562–565. [http://doi.org/10.1016/S0257-8972\(03\)00081-1](http://doi.org/10.1016/S0257-8972(03)00081-1)
- Lee, S.M., Murakami, H., & Ito, T. (2001). Properties of thin MgO films grown on single-crystalline CVD diamond, *Applied Surface Science*, 175–176, 517–524. [http://doi.org/10.1016/S0169-4332\(01\)00105-2](http://doi.org/10.1016/S0169-4332(01)00105-2)
- Kobayashi, S., (2010). X-ray thin-film measurement technique IV. In-plane XRD measurements. *The Rigaku Journal*, 26, 3–11.
- Mitsunaga, T. (2009). X-ray thin-film measurement technique II. Out-of-plane diffraction measurements. *The Rigaku Journal*, 25, 7–12.

- Chudzik, M.P., Koritala, R.E., Luo, L.P., Miller, D.J., Balachandran, U., & Kannewurf, C.R., (2001). Mechanism and processing dependence of biaxial texture development in magnesium oxide thin films grown by inclined-substrate deposition, *Applied Superconductivity. IEEE Transactions on*, *11*, 3469–3472. <http://doi.org/10.1109/77.919810>
- Maksimov, O., Fisher, P., Skowronski, M., Salvador, P. A., Snyder, M., Xu, J., & Weng, X. (2008). MgO films grown on yttria-stabilized zirconia by molecular beam epitaxy. *Journal of Crystal Growth*, *310*, 2760–2766. <http://doi.org/10.1016/j.jcrysgro.2008.02.013>
- Cho, J.-M., Lee, K.-H., Cheon, C. I., Cho, N. I., & Kim, J. S. (2010). Characterization of the biaxial textures of MgO thin films grown by E-beam evaporation. *Journal of the European Ceramic Society*, *30*, 481–484. <http://doi.org/10.1016/j.jeurceramsoc.2009.06.015>
- Kopp, V.S., Kaganer, V.M., Jenichen, B., & Brandt, O. (2014). Analysis of reciprocal space maps of GaN(0001) films grown by molecular beam epitaxy. *Journal of Applied Crystallography*, *47*, 256–263. <http://doi.org/10.1107/S1600576713032639>
- Hwang, K.-S. (1998). Reciprocal-space mapping studies of Pb(Zr,Ti)O<sub>3</sub> thin films grown by the spin-coating technique. *Journal of the Korean Physical Society*, *33*, 476–479.
- Kennedy, R. J., & Stampe, P. A. (1999). Reciprocal space mapping of epitaxial MgO films on SrTiO<sub>3</sub>. *Journal of Crystal Growth*, *207*, 200–205. [http://doi.org/10.1016/S0022-0248\(99\)00371-1](http://doi.org/10.1016/S0022-0248(99)00371-1)

### Copyrights

Copyright for this article is retained by the author(s), with first publication rights granted to the journal.

This is an open-access article distributed under the terms and conditions of the Creative Commons Attribution license (<http://creativecommons.org/licenses/by/3.0/>).